PCCP
Physical Chemistry Chemical Physics

Accepted Manuscript

This article can be cited before page numbers have been issued, to do this please use: P. Pertierra, M. A. Salvadó, R. Franco and J. M. Recio, *Phys. Chem. Chem. Phys.*, 2022, DOI: 10.1039/D2CP01266A.

ROYAL SOCIETY OF CHEMISTRY

rsc.li/pccp

View Article Online
DOI: 10.1039/D2CP01266A

PCCP

ARTICLE TYPE

Cite this: DOI: 00.0000/xxxxxxxxxx

Pressure and temperature stability boundaries of cubic SiC polymorphs: a first-principles investigation

Pilar Pertierra, Miguel A. Salvadó*, Ruth Franco and J. Manuel Recio

Received Date
Accepted Date

DOI: 00.0000/xxxxxxxxxx

A better understanding of the effects of thermal and pressure on the wide gap SiC semiconductor is necessary for both (i) an improvement of the performance of this compound in a variety of technological applications and (ii) the clarification of controversial issues related to the stability of its cubic polymorphs at high pressure and high temperature. Bearing in mind this double demand, we perform first-principles calculations of the phonon band structures, vibrational density of states, and thermal and mode Grüneisen parameters of the zinc blende (B3) and rock-salt (B1) cubic polymorphs of 3C-SiC covering pressures and temperatures up to 120 GPa and 3000 K, respectively. Under a martensitic description of the B3-B1 transformation, we found that the large hysteresis pressure range observed at room temperature (35 GPa-100 GPa) vanishes around 1100 K. The calculated Clapeyron slope of this transformation is slightly negative, with an average value of -2.9 MPa/K in the 0-3000 K interval and -3.7 MPa/K at 2000 K. We also study the decomposition reaction of the two cubic polymorphs into their elemental constituents (C, Si) finding a decreasing (increasing) decomposition temperature for the B3 (B1) phase as pressure is applied. All these results are sustained by a good agreement with other recently reported experimental and theoretical thermodynamic data that have been also evaluated under our quasi-harmonic approximation framework.

1 Introduction

Besides being a fundamental constituent of proposed C-rich exoplanets with implications in the C-life cycle[1,2], SiC gathers many demanded properties related to its high stability when operating at hostile pressure and temperature conditions (see for example Refs.[3] and[4]). The outstanding performance of the hexagonal and cubic SiC polytypes is continuously highlighted in numerous publications due to their extensive applications in such diverse fields as power electronics[5], quantum spintronics[6], manufacturing of abrasive tools[3], aerospace industry[7] or nuclear energy[8].

The fabrication processes of SiC polytypes have been a concomitant matter of continuous developments within these fields requiring further investigation[9]. La Via *et al.*[4] put the emphasis on the singularities of the cubic zinc blende polymorph (3C-SiC-B3) as it is the only one growing on Si wafers. Drawbacks of this heteroepitaxial process are also remarked since the mismatch between the lattice spacings in 3C-SiC-B3 (a = 4.36 Å) and Si (a = 5.43 Å) introduces undesired strains and subsequent stacking faults and defects in the cubic polymorph[4,10–12]. The apparition of the so-called thermoelastic stress due to a difference of around 8% between the thermal expansion coefficients of 3C-SiC-B3 and Si is also pointed out[4,10,11,13]. The relevance of these limitations clearly illustrates the importance of disposing a precise knowledge of how temperature affects the interatomic distances of this cubic SiC polymorph.

Along with temperature, pressure introduces desired strains in materials if it is appropriately controlled. Both together, pressure and temperature, have been the subject of a recent investigation exploring the onset of the plastic behaviour in 3C-SiC-B3 samples under pressures and temperatures up to 7.4 GPa and 1400 °C, respectively[3]. Besides the conclusion of its superior mechanical performance when compared with the most popular strongest materials (diamond, moissanite or α-Si_3N_4), the 'much higher pressure and temperature requirements for phase transition and decomposition' of 3C-SiC-B3 were also remarked[3].

However, the limits associated with the pressure-induced B3-B1 (rocksalt) phase transition and the decomposition of 3C-SiC into its elemental constituents are a matter of debate showing a number of discrepancies in the publications reported so far. For example, Miozzi *et al.*[2] 'do not observe any decomposition of SiC compound or change in diffraction peaks intensity over 2000 K, in the pressure range 30–60 GPa' in opposition to a previous experimental work of Daviau and Lee[14]. These two authors have later critically examined the factors producing the differences in the observations noticing that the interplay of thermodynamic and

MALTA-Consolider Team and Departamento de Química Física y Analítica, Universidad de Oviedo. E-33006 Oviedo, Spain
*Corresponding author; E-mail: mass@uniovi.es

View Article Online
DOI: 10.1039/D2CP01266A

kinetic effects makes the stability boundaries of these two polymorphs to depend on the particular conditions of the experiments (static or dynamic compression, rate of increasing temperature and pressure, etc.) and the history of the sample [15]. Our previous investigation on the B3-B1 transition path in 3C-SiC [16] has also contributed to clarify how the own process of cooling/heating and loading/unloading pressure is determinant to decide which will be the (meta)stable phase observed at the final achieved pressure and temperature of the sample.

Our view of this reconstructive B3-B1 transition does not take into account the well-known mechanical stability criteria (involved in displacive transformations) recently applied by Ran *et al.* [17], since the energetic barriers and the hysteresis of the transformation are here the key factors affecting the observed pressure values for the direct and reverse B3-B1 transitions. Overall, computer simulations are at this regard very convenient since they can separate thermodynamic boundaries (usually less complicated to evaluate) from kinetic effects involving transition mechanisms and time evolution of atomic displacements (see the two first chapters of Ref. [18]).

The increasing technological interest in SiC and the controversial experimental and theoretical data have drawn us to carry out a computational study directed to the accurate determination of the structural and stability behavior of SiC cubic polymorphs under different temperature and pressure conditions. Pressure-Volume-Temperature (p-V-T) data were obtained from first-principle density functional theory (DFT) calculations involving the evaluation of phonon dispersion curves under the quasi-harmonic approximation (QHA). Our recent results on the B3-B1 transition mechanism [16] have been further exploited using these new QHA calculations to evaluate energetic barriers associated with the direct and inverse transitions at different pressures and temperatures.

Our focus is on (i) the hysteresis associated with the B3-B1 pressure-induced phase transition, (ii) the sign of the slope of the Clapeyron equilibrium curve of this transition, and (iii) the stability of SiC against its decomposition into its elementary C and Si constituents. We first provide thermal EOS parameters of B3 ($F\bar{4}3m$) and B1 ($Fm\bar{3}m$) SiC polymorphs, with special emphasis on the rock-salt phase since it is not observed at zero pressure. Second, the narrowing of the pressure hysteresis range is determined from 0 K to around 1100 K, where it vanishes. Third, our calculations allow us to estimate a slightly negative Clapeyron slope for the B3 $\rightarrow$ B1 transition that increases in absolute value as temperature increases. Finally, we find that the decomposition of 3C-SiC into stable Si and C polymorphs at high temperature and high pressure shows different trends for the B3 and B1 phases.

The rest of our contribution is split into three more sections. Section 2 contains information about our computational procedure and the parameters used in the calculations. Results are discussed in two different subsections. The first one is devoted to the static and thermal equations of state of 3C-SiC B3 and B1 polymorphs, whereas the second deals with their own stability, with respect to each other, and against decomposition into C and Si. The paper ends with a summary of the main findings.

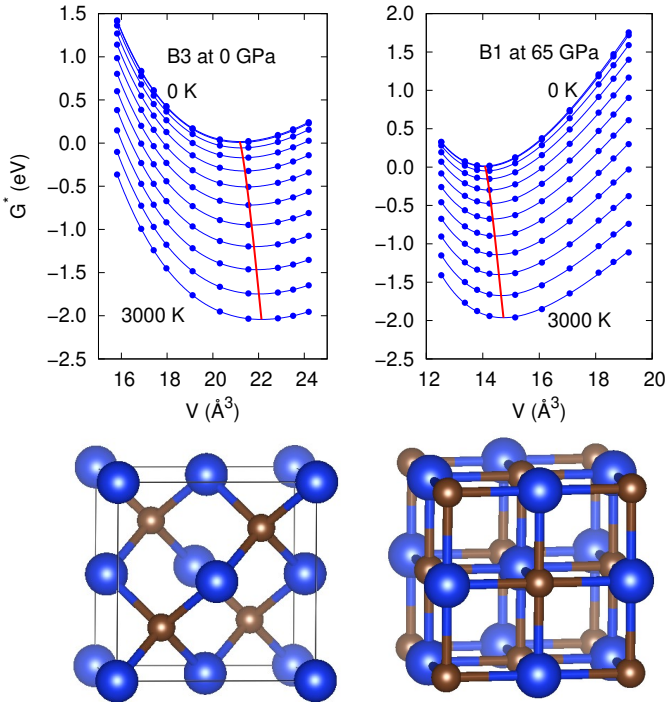

Fig. 1 Gibbs energy *vs* volume data points from 0 K to 3000 K, at 250 K intervals (top), for B3 at 0 GPa (left) and for B1 at 65 GPa (right) according to our quasi-harmonic calculations. Red lines join minima of the third-order Birch-Murnaghan fitting curves (in blue). At the bottom, structure representations of the respective phases.

2 Computational Details

Density functional perturbation theory (DFPT) calculations under the generalized gradient approximation (GGA) were carried out using the VASP code [19] at selected volumes of both B3 and B1 3C-SiC polymorphs (see unit cells of both structures in Fig. 1). A 2×2×2 supercell of the corresponding conventional unit cells was chosen. We used the Perdew-Burke-Ernzerhof (PBE) exchange-correlation functional [20] and k-point Γ-centered Monkhorst-Pack meshes [21] where the numbers of subdivisions along each reciprocal lattice vector $\vec{b}_i$ were given by $N_i = \max(1, 90 \times |\vec{b}_i| + 0.5)$ along with an energy cutoff of 600 eV. The projector-augmented wave (PAW) method was included to account for the interaction between the valence and the core electron densities [22,23]. Thermal contributions were included within the QHA framework implemented in the `Phonopy` package [24]. A 41×41×41 q-point mesh was used for the calculations of the phonon dispersion curves. Thermal energies at selected pressure-temperature pairs were calculated using our home-made `Gibbs2` code [25,26], that easily allows the calculated `Phonopy` phonon density of states (DOS) at each volume to be introduced as input data. For the phonon dispersion bands plots and mode Grüneisen parameters calculation, a non-analytical term correction was included. In the calculation of C-diamond and Si-hcp, a 2×2×2 and 4×4×2 supercells were chosen respectively.

View Article Online
DOI: 10.1039/D2CP01266A

3 Results and Discussion

3.1 Static and Thermal EOS

Fig. 1 shows our calculated (G_i^*-V_i) data points at selected temperatures from 0 K to 3000 K for the B3 polymorph at zero pressure and for the B1 phase at 65 GPa. G_i^* is $F_i^*(V_i;T) + pV_i$ and, therefore, the Gibbs energy (G) becomes the Helmholtz energy (F) at zero pressure. The star superscript refers to the so-called non-equilibrium G and F free energies[26]. The minima of these curves determine the equilibrium volumes and energies corresponding to each of the given pressure and temperature values. A third-order Birch-Murnaghan analytic equation of state (EOS) is used to describe the calculated (G_i^*-V_i) data points. At zero pressure the equilibrium volumes obtained correspond to cell parameter values of 4.380 Å for B3 and 4.058 Å for B1. Similar calculations were carried out at selected pressures up to 120 GPa. From these fittings, p-V-T equilibrium values and the corresponding EOS parameters were extracted.

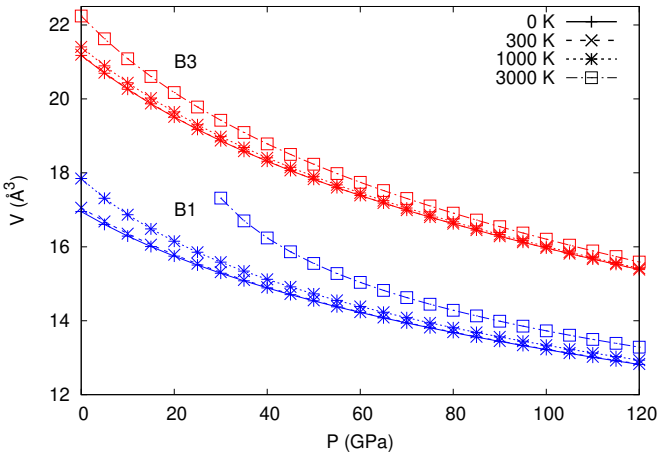

Fig. 2 Calculated thermal EOS for B3 and B1 polymorphs.

In Fig. 2, the p-V calculated equations of state of B3 and B1 phases at 0 K, 300 K, 1000 K, and 3000 K are displayed. Thermal contributions have been incorporated after evaluating the phonon dispersion curves (see later) under the QHA. As T increases, the expected increasing compressibility of both polymorphs is revealed in these plots by the progressive greater slopes of the curves from 0 K to 3000 K (more difficult to appreciate for the B3 phase). This trend is quantified in Fig. 3, where the temperature evolution of the corresponding zero pressure bulk moduli (B_0) at 0, 65, and 120 GPa is plotted. The negative slope observed in the B_0 *vs* T graphs of Fig. 3 is greater (in absolute value) in the B1 case. For the B3 phase, a low $\left(\frac{\partial B_0}{\partial T}\right)_p$ value of -0.037 GPa/K was measured by Wang *et al.*[27] (-0.014 GPa/K from DFT calculations) who remarked the high thermal stability of this B3 phase. We confirm this result that contrasts with the behavior of the B1 phase which shows severe phonon softening at 0 GPa and high temperatures.

Our calculated B_0 values for B3 and B1 at 300 K are 207 GPa and 216 GPa, respectively, 212 and and 243 are the corresponding static values, and 208 and 230 are the values at 0 K including thermal zero-point corrections. The static calculated B_0 values

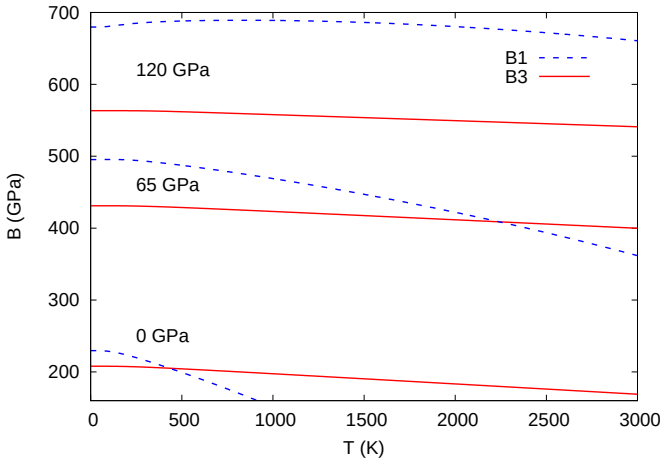

Fig. 3 Calculated temperature evolution of bulk moduli of B3 and B1 SiC polymorphs at 0, 65, and 120 GPa.

for B3 and B1 are inside the range of other analogous calculations[28–34]. At 300K, our calculated B_0 value for B3 is similar to the value calculated (GGA, quasi-harmonic) by Kidokoro *et al.*[33]. Both are slightly below the smallest reported experimental values[1,2,27,35–37] including the own measurement of Kidokoro *et al.* For B1 at 300 K, our calculated B_0 value is smaller than the value calculated by Kidokoro *et al.*[33] by a 10% and than the value measured by the same authors by a 8%. These results are within the expectations since GGA usually predicts crystals more compressible than the observed ones. A considerably higher value (323 GPa) was measured by Miozzi *et al.* for the B1 phase[2]. It should be noted that in this experimental determination of B_0 only pressures values above 50 GPa were used. This fact can lead to a large uncertainty in the determination of the EOS parameters at zero pressure since the zero pressure volume (V_0) is a non-linear parameter in the fitting procedure.

The thermal expansion coefficient (α) of both phases at different pressures was also evaluated under the quasi-harmonic approximation. Our α value for 3C-SiC-B3 at zero pressure and 300 K (8.15×10^{-6} K^{-1}) is close to the experimental value[27,38] and previous computations[27,39]. The value of α reduces with pressure at a progressively decreasing rate (in absolute value) with an estimated average derivative -2.14×10^{-7} K^{-1} GPa^{-1} between 0 and 5 GPa and -0.97×10^{-7} K^{-1} GPa^{-1} between 0 and 65 GPa. We notice that the accurately determined α value of Si at room T (7.71×10^{-6} K^{-1} [13]) is already reached by 3C-SiC-B3 at around 2 GPa according to our calculations. Zielinski *et al.*[10] and Iacopi *et al.*[11] pointed out that the mismatch between the thermal expansion coefficient of 3C-SiC-B3 and Si is one of the factors introducing an undesired residual strain preventing a good growth of 3C-SiC films. Although other factors as the specific plane of the Si substrate and the orientation growth[11] (beyond the scope of our study) are key to improve the deposition process, we notice that the combined role of pressure and temperature can be used to approach both expansion coefficients.

On the other hand, the B1 phase has an α value about five times greater than that of the B3 phase at 0 GPa (41.9×10^{-6} K^{-1}). It also decreases with pressure and about the transition

View Article Online
DOI: 10.1039/D2CP01266A

pressure (∼65 GPa, see below) has for B1 a value similar to B3 at zero pressure. The greater value of α in the B1 phase can be explained as due to a consequence of larger nearest neighbor distances caused by the increasing in the coordination number in this phase which leads to lower frequencies for the high-pressure phase (see below) and a subsequent greater thermal expansion parameter. It is to be remarked that, in contrast with $\left(\frac{\partial B_0}{\partial T}\right)_p$, $\left(\frac{\partial \alpha}{\partial p}\right)_T$ is very similar for both B3 and B1 polymorphs. We concluded that, as regards these thermoelastic properties, temperature discriminates both phases but pressure does not. Nisr *et al.*[1] measure the combined effect of pressure on the thermal expansion of B3 at a temperature as high as 2500 K. They obtain values for α in the range $1.5-2.0\times10^{-5}$ K^{-1} (compared with our calculated values: 2.02×10^{-5} K^{-1} at 0 GPa and 6.37×10^{-6} K^{-1} at 100 GPa). Their reported values of α with pressure depends on the gold scale used for pressure. Whereas using Ref. 40 scale, α is nearly constant, with the Ref. 41 scale, α decreases significantly with pressure in a somewhat lesser extent that our calculations, but more consistently with them.

3.2 Phase stability

3.2.1 Phonon dispersion curves and dynamical stability

Before analyzing the pressure and temperature regions where our calculations detect the presence of (meta)stable B3 or B1 polymorphs, we focus on the inherent dynamical stability of the two phases. The presence of imaginary frequencies in the optical modes of the phonon dispersion curves are indicative of a dynamical unstable structure and provides a complementary analysis to the mechanical stability criteria based on Born's elastic constants relationships[42].

Phonon dispersion curves and the vibrational density of states for the two phases at two pressures are shown in Fig. 4. For B3 our results are in overall agreement with the experimental phonon dispersion data (at room conditions) collected in Ref. 43. Our results can be compared also with the theoretical results (for B3 and B1) of Thakore *et al.*[44]. In agreement with these authors, we have found in the B3 phase that the frequency is lowered with pressure along the directions Γ-K and Γ-L but this change is small and, according to our calculations, if the pressure is increased above 70 GPa, it does not progresses significantly. Our results for this phase agree also with the observations and comments about phonon softening around 40 GPa reported in Ref. 37. In the B1 spectra, we do not observe imaginary frequencies up to volumes corresponding to temperatures around 1500 K at 0 GPa, although some of the frequencies, including optical ones decrease notably. We conclude that B1 is dynamically stable at room conditions. The same result was obtained in the calculations of Ivashchenko *et al.*[45]. Therefore, we confirm the possibility of having the B1 polymorph at zero pressure if temperature is low enough.

Not evidence of dynamic instabilities were found in either of the two phases up to 100 GPa. Recent results of Ran *et al.*[17] based on explicit elastic constants calculations showed a mechanical instability of B3 phase at 112 GPa. Although the impossibility of even a metastable 3C-SiC-B3 phase at pressures above 112 GPa is deduced from these calculations, we would like to make clear that we have not found any indications relating this instability with a softening mechanism involved in the B3 to B1 transition, what is not surprising in the context of a reconstructive transition.

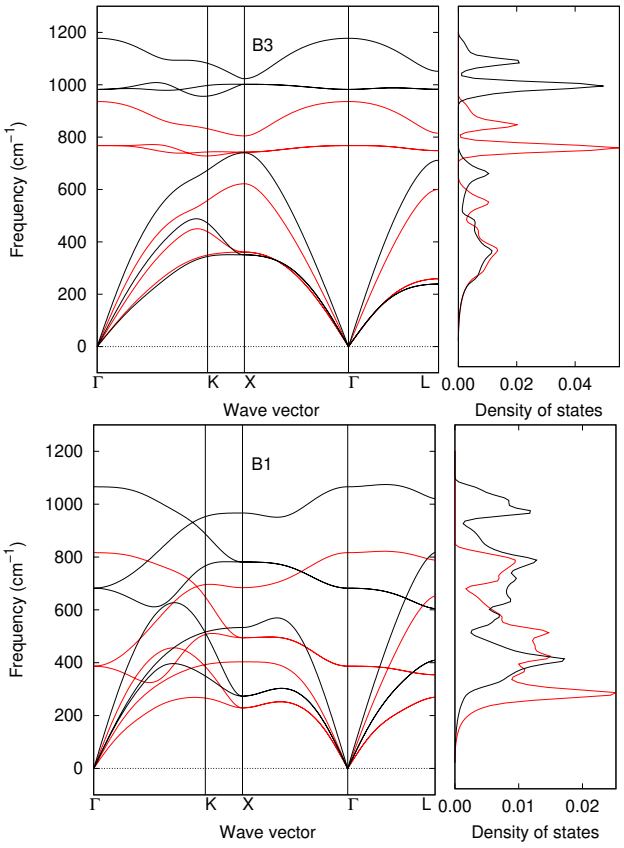

Fig. 4 (Top) Phonon dispersion curves and density of states of B3-SiC at 0 GPa (red) and 71 GPa (black). (Bottom) Phonon dispersion curves and density of states of B1-SiC at 0 GPa (red) and 71 GPa (black).

Information of how the phonon frequencies evolve as the unit cell volume changes with T and p is enclosed in the modal Grüneisen parameters. The most representative ones are gathered in Table 1. For the B3 phase, our results for TO(Γ) and LO(Γ) are in agreement with previous calculations and experimental results[37,39,46–53]. Outside the Γ point the only experimental results available are from Wang *et al.*[52], that were obtained using the data of Olego *et al.*[46,47] but assuming the own Wang *et al.* theoretically calculated bulk modulus. The overall agreement we found with respect to the experimental results (except for LA(L)) provides support to our data outside those ranges that are not available in other calculations and experiments. Softening has been observed or predicted for the B3 phase for the modes and points TA(L)[52], LA(L)[52] and TA(X)[39,48]. In our results, softening is predicted at 0 GPa in TA(L) and in both TA(L) and TA(X) at higher pressures. For LA(L) our values are clearly non-negative in the range studied. These calculated negative mode Grüneisen parameters in the B3 phase for the TA modes at X and L special points could be interpreted as a signal for a potential dynamical instability but our phonon calculations at high pressure discussed

View Article Online
DOI: 10.1039/D2CP01266A

Table 1 Calculated mode Grüneisen parameters of the B3 and B1 SiC polymorphs. In each pair of numbers, the first corresponds to 0 GPa and the second to 71 GPa.

	B3			B1		
	Γ	L	X	Γ	L	X
LO	1.09, 1.02	1.15, 1.16	1.15, 1.05	1.59, 1.25	1.54, 1.20	1.47, 1.79
TO	1.14, 1.11	1.30, 1.20	1.45, 1.29	4.32, 2.21	2.72, 2.39	3.25, 2.01
LA	-	0.96, 0.66	0.82, 0.78	-	3.58, 0.90	2.07, 0.97
TA	-	-0.10, -0.71	0.14, -0.45	-	1.44, 1.80	0.99, 1.73

above does not confirm this hypothesis. At this respect, it is interesting to note that the presence of negative mode Grüneisen parameters in other zinc-blende (B3) and diamond-like semiconductors is considered as a necessary condition for the presence of negative thermal expansion at low temperature[54] although a study of this phenomenon in SiC is out of the scope of the present work.

3.2.2 Hysteresis and Clapeyron slope

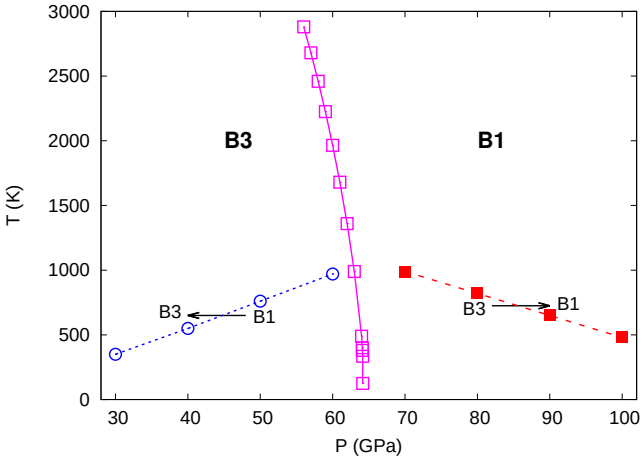

Fig. 5 Temperature dependence of transition pressures fulfilling the thermodynamic equilibrium condition $\Delta G = 0$ (solid line). Temperature dependence of pressures needed to overcome the kinetic barrier for the direct B3 → B1 (red, dotted line) and the inverse B1 → B3 (blue, dotted line) transition.

Let us now summarize the data reported so far concerning the pressure-induced B3-B1 phase transition (see also Ref. 15 for more details). Yoshida *et al.*[36] found experimentally values of 100 GPa and 35 GPa at room temperature for the direct B3 → B1 and inverse B1 → B3 transitions, respectively, whereas the calculations available at that time ([28,49,55]) predicted the B3-B1 phase equilibrium at around 60 GPa. Daviau and Lee[56] observed a transition pressure (p_T) around 64.5±2.1 GPa when the sample was heated at temperatures around 1500-1700 K, very close to the calculated pressures predicted in the theoretical studies above and also in other reported later[16,28–30,32,57–59]. Kidokoro *et al.*[33] informed of a slightly higher experimental value of 74 GPa at 2100 K, whereas their calculations using the quasi-harmonic approximation at the GGA level gave a value of 60 GPa at that temperature, 65 GPa at 0 K and 67 GPa when zero pressure contributions were also neglected (static conditions). The most recent static compression experiments of Miozzi *et al.*[2] surprisingly 'place the transition at 66 ± 2 GPa at room temperature and between 65 and 70 GPa at high temperature'.

In a previous study[16], we calculated a static transition pressure of 66 GPa and estimated using a simple kinetic model a transition pressure of 110 GPa at 300 K. In order to evaluate the pressure hysteresis range of the B3-B1 transformation, the vibrational energies of the B3 and B1 phases at different pressures and temperatures have been calculated using now the phonon dispersion curves evaluated under the quasi-harmonic approximation instead of a simple Debye model (see details in Ref. 16). The transition temperature-pressure values are depicted in Fig.5 for the direct B3 → B1 (red dotted lines) and B1 → B3 (blue dotted lines). With a few exceptions (mainly the last values of Miozzi *et al.*[57]), it is possible to reconcile the variety of experimental and theoretical data using our results since they take into account the thermodynamic and kinetic factors affecting the transition.

Most of the calculated values for the transition pressure are around 65 GPa. As they are evaluated requiring equal Gibbs energy (or enthalpy at static conditions) for both phases, they represent an ideal thermodynamic boundary. These thermodynamic predictions should be compared with the pressure at the onset of the high-pressure phase only in high temperature experiments where the sample has enough thermal energy to overcome the kinetic barrier associated with the transition. For that reason, the theoretical predictions are in good agreement with the value of Daviau and Lee[56] and to a less extent with Kidokoro *et al.*[33]. Other factors related to the purity of the sample, hydrostaticity of the transmitting medium, rate of the pressure load, etc. can affect the observation of the high-pressure phase and may explain the unexpected low transition pressure found by Miozzi *et al.* at room temperature[2].

In addition, the results plotted in Fig. 5 also account for the hysteresis range (35 GPa, 100 GPa) at room temperature reported by Yoshida *et al.*[36]. Considering the success of this simple kinetic model, we can delimit the presence of the two polymorphs at different pressure and temperature conditions using the diagram of Fig. 5. Above (below) the red (blue) dotted line only the B1 (B3) would be expected, whereas in between these two dotted lines the actual observed polymorph depends on whether we are loading (B3) or unloading (B1) pressure.

As regards the Clapeyron $\frac{dp_T}{dT}$ slope, although there are less experimental and theoretical data, the existing discrepancies have also received particular attention lately. Daviau and Lee gathered the most relevant results in Fig. 3 of Ref. 15. Using their experimental results and those of Yoshida *et al.*[36], they found a slope for the B3-B1 boundary of -26.4±3.9 MPa/K using three p_T-T points and of -19.4±0.32 MPa/K using two p_T-T points. They remarked that their values can be excessively large due to the kinetic effects

View Article Online
DOI: 10.1039/D2CP01266A

involved in this transition. In fact, they also applied an approximated model derived by Li and Jeanloz[60] to get rid of the kinetic effects and obtained an almost negligible dependence of the transition pressure on T. Their estimations vary from a positive $+1.8$ MPa/K to a negative -0.7 MPa/K Clapeyron slope[56]. Kidokoro *et al.*[33] recognized the difficulties of an experimental determination of this slope and reported calculated (GGA, quasi-harmonic) values that increase (in absolute value) from -1.3 MPa/K at 500 K to -4.0 MPa/K at 2000 K. On the other hand, the static compression experiments of Miozzi *et al.*[2] inform of a small but positive Clapeyron slope of $+1$ MPa/K.

The comparison between experimental and theoretical Clapeyron slopes should be carried out with care since temperature affects both the thermodynamic equilibrium position ($\Delta G = 0$, $\Delta G = \Delta H - T\Delta S$, ΔH and ΔS are, respectively, the change of enthalpy and entropy associated with the transition) and the kinetics of the transformation. Once we plot the variation of our calculated ΔG values with pressure at different temperatures (see Fig. 6), we observe an overall decreasing of the transition pressure with T. The corresponding values go from 64.1 GPa at 0 K to 55.3 GPa at 3000 K, leading to an average Clapeyron slope of -2.9 MPa/K in this interval and -3.7 MPa/K at 2000 K. These results follow the same trend and are of the order of the ones found by Kidokoro *et al.*[33]. The effect of T on the kinetic barriers is obvious: the higher the temperature the more the vibrational energy available to overcome the barrier and therefore the lower the observed transition pressure (see also the dotted red line in Fig. 5). Thus, according to our calculations, the overall effect of increasing the temperature is to decrease the transition pressure.

This result can be supported by an argument similar to the one stated by Kidokoro *et al.*[33]. Since $\frac{dp_T}{dT} = \frac{\Delta S}{\Delta V}$ and ΔV is negative for a reconstructive pressure-induced phase transition, the sign of the Clapeyron slope depends on the entropy change across the transition. Usually, this change is close to zero for a solid-solid transition. In this case, the high-pressure B1 phase has a higher Si and C atomic coordination (six-fold) than the B3 one (four-fold) with larger Si-C nearest neighbour distances and overall lower frequencies. This leads to a greater number of available energetic vibrational levels for a given temperature in the high-pressure B1 phase and, therefore, a greater entropy than in the B3 low-pressure phase. As a result, a negative Clapeyron slope is expected in agreement with the calculations.

3.2.3 SiC decomposition

In order to study the influence of hydrostatic pressure on the temperature decomposition of SiC, we have modelled this process using for the elements the diamond and hcp polymorphs of carbon and silicon, respectively. The hcp-Si polymorph is assumed to be the stable phase of silicon between 42 and 79 GPa[61]. When we add the Gibbs energy of Si and C and compare the total value with respect to that of the B3 and the B1 phases of SiC, we observe that the thermodynamic decomposition of the compound is predicted for the B3 phase at around 1300 K at 50 GPa and only at a slightly greater temperature (1380 K) for the B1 phase at 70 GPa. Daviau and Lee[14] reports a decomposition temperature for the B3 phase of around 2000 K at 60 GPa and no decompositon of B1 phase at

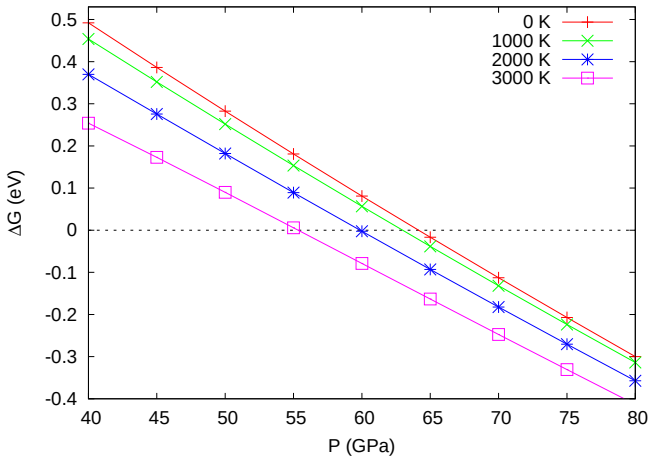

Fig. 6 Gibbs energy of the B1 phase with respect to the B3 one (dotted line) calculated at 0 K, 1000 K, 2000 K, and 3000 K.

3200 K and 80 GPa. It should be beard in mind that the melting point of silicon is probably around 2000 K at 60 GPa[62] and then, our decomposition predictions at high T are limited by the validity of the quasi-harmonic approximation. It should also be noted that in the hcp-Si thermal calculations at high volumes part of the frequencies were imaginary and they were not included in the subsequent calculations. For silicon, when high pressure is combined with enough high temperature the stable phase is probably fcc[63]. Further research in this direction is needed to fully address the complexity of SiC decomposition.

It may be of interest in the synthesis of 3C-SiC to remark the different behaviour that we have found for the two cubic polymorphs as regards the influence of pressure on their decomposition temperatures. For the B3 phase, an increasing in pressure leads to a lower decomposition temperature in our calculations (red lines in Fig. 7). This is in qualitative agreement with the experimental observations of Daviau and Lee[14] that reported a negative phase boundary for this solid reaction. Our results are consistent with the known stability of 3C-SiC-B3 at high temperature and ambient or low pressure and quantify that this trend is by about -8 K/GPa. For the B1 phase, we have found an opposite trend. At 100 GPa, the decomposition temperature is around 470 K higher that at 70 GPa (blue lines in Fig. 7). These results are well explained recalling to the pressure stability regions of both B3 and B1 phases. We have seen that in 3C-SiC the packing efficiency with Si and C six-fold coordinations is preferred at high pressure. This behavior makes the temperature decomposition of the B1 phase to be higher as pressure increases for this phase. The same trend does not apply for the B3 phase because pressure tends to destabilize the 4-fold Si and C coordination of this structure and contributes to the decomposition of SiC at high temperature.

4 Conclusions

Due to the increasing interest of SiC polytypes in a variety of applications at an every day more demanding conditions, we have explored the pressure and temperature regions where 3C-SiC can be found stable or metastable in the form of zinc blende (B3)

View Article Online
DOI: 10.1039/D2CP01266A

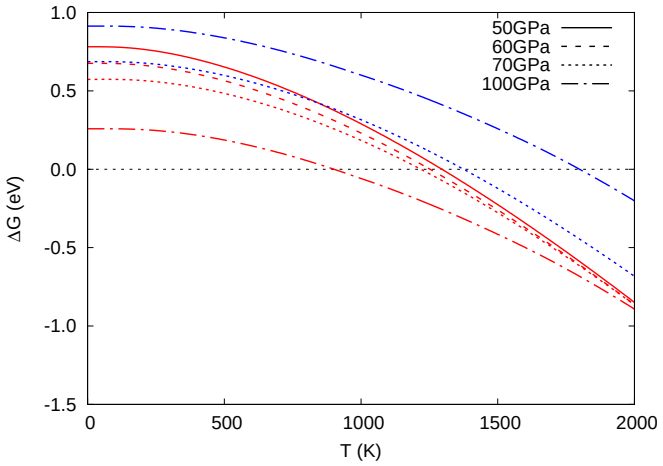

Fig. 7 Calculated Gibbs energy of Si(hcp) and C(diamond) with respect to the B3 (red) and B1 (blue) polymorphs of SiC at different pressures and temperatures.

or rocksalt (B1) polymorphs. As expected, both phases show less compressibility as pressure increases and are more compressible as temperature increases. It is noticeable to observe the existence of a crossing point between our B3 and B1 calculated $B_0 - T$ curves that informs of a greater thermal stability of the B3 phase. This result is more evident at low pressure (B1 shows severe phonon softening at 0 GPa if temperature increases above 1000 K) and turns to change if pressure increases above 100 GPa where the B3 phase shows mechanical instability above 110 GPa. Our calculations predict a thermal expansion coefficient for the B1 phase five times greater than for the B3 phase. Both decrease with pressure at a similar rate leading for the B3 phase a value similar to the one of Si at room temperature at only 2 GPa. This results has implications on the heteroepitaxial growth of 3C-SiC-B3 films using Si as a compliance substrate.

To make clear our contribution, we would like to specifically point out the main findings of our investigation. To begin with, the thermodynamic B3-B1 transition pressure at 300 K has been predicted around 64 GPa. We have also emphasized that to compare with data obtained in a variety of experiments, kinetic effects have to be taken into account too. We were able to evaluate the energetic barriers associated with the direct and reverse transitions and, therefore, we have quantified how pressure hysteresis ranges decrease from 82 GPa at room temperature (28 GPa-110 GPa) to 7 GPa at 1000 K. These results allow us to reconcile many of the previous reported data. Similarly, the Clapeyron slope of the B3-B1 boundary was found to show a slightly negative slope with a value around -3 MPa/K in the 0-3000 K range if phase equilibrium is considered. However, a higher negative value is obtained when the kinetic effects present in the experiments are involved in the calculation. Our results shed light on the sign of the Clapeyron slope, given the discrepancies observed between some recent experimental results[2,56]. Finally, although our predictions concerning the stability of SiC cubic polymorphs against decomposition into hcp-Si and C-diamond are affected by the limitations of the quasi-harmonic approximation at high temperature, we were also able to provide a reasonable account of the different response of the two polymorphs. According to our investigation, B3 shows a negative temperature decomposition rate with pressure, whereas an opposite trend is found for the B1 phase that needs higher temperature to decompose if pressure increases.

Conflicts of interest

There are no conflicts to declare.

Acknowledgements

This work was supported by Spanish MCIU and MINECO through the following projects: PGC2018-094814-B-C2 and RED2018-102612-T. MALTA-Consolider supercomputing center is gratefully acknowledged.

Notes and references

1 C. Nisr, Y. Meng, A. A. MacDowell, J. Yan, V. Prakapenka and S.-H. Shim, *J. Geophys. Res. Planets*, 2017, **122**, 124–133.
2 F. Miozzi, G. Morard, D. Antonangeli, A. N. Clark, M. Mezouar, C. Dorn, A. Rozel and G. Fiquet, *J. Geophys. Res. Planets*, 2018, **123**, 2295–2309.
3 Y. Wang, *AIP Advances*, 2020, **10**, 065209 [1–5].
4 F. La Via, M. Zimbone, C. Bongiorno, A. La Magna, G. Fisicaro, I. Deretzis, V. Scuderi, C. Calabretta, F. Giannazzo, M. Zielinski, R. Anzalone, M. Mauceri, D. Crippa, E. Scalise, A. Marzegalli, A. Sarikov, L. Miglio, V. Jokubavicius, M. Syväjärvi, R. Yakimova, P. Schuh, M. Schöler, M. Kollmuss and P. Wellmann, *Materials*, 2021, **14**, 5348 [1–35].
5 T. P. Chow, *Microelectron. Eng.*, 2006, **83**, 112–122.
6 N. T. Son, C. P. Anderson, A. Bourassa, K. C. Miao, C. Babin, M. Widmann, M. Niethammer, J. Ul Hassan, N. Morioka, I. G. Ivanov, F. Kaiser, J. Wrachtrup and D. D. Awschalom, *Appl. Phys. Lett.*, 2020, **116**, 190501 [1–7].
7 G. N. Bullen, *SAE Int. J. Aerosp.*, 2014, **7**, 146–155.
8 E. López-Honorato, J. Tan, P. Meadows, G. Marsh and P. Xiao, *J. Nucl. Mater.*, 2009, **392**, 219–224.
9 S. Daoud, N. Bouarissa, H. Rekab-Djabri and P. K. Saini, *Silicon*, 2021, https://doi.org/10.1007/s12633–021–01387–8.
10 M. Zielinski, S. Ndiaye, T. Chassagne, S. Juillaguet, R. Lewandowska, M. Portail, A. Leycuras and J. Camassel, *Phys. Status Solidi A*, 2007, **204**, 981–986.
11 F. Iacopi, G. Walker, L. Wang, L. Malesys, S. Ma, B. V. Cunning and A. Iacopi, *Appl. Phys. Lett.*, 2013, **102**, 011908.
12 K. Kim, S. Son, S. Lee, J.-H. Ahn and Z. Lee, *Cryst. Growth Des.*, 2022, **22**, 1421–1426.
13 H. Watanabe, N. Yamada and M. Okaji, *Int. J. Thermophys.*, 2004, **25**, 221–236.
14 K. Daviau and K. K. M. Lee, *Phys. Rev. B*, 2017, **96**, 174102 [1–10].
15 K. Daviau and K. K. M. Lee, *Crystals*, 2018, **8**, 217 [1–18].
16 M. A. Salvadó, R. Franco, P. Pertierra, T. Ouahrani and J. M. Recio, *Phys. Chem. Chem. Phys.*, 2017, **19**, 22887–22894.
17 Z. Ran, C. Zou, Z. Wei, H. Wang, R. Zhang and N. Fang, *Ceram. Int.*, 2021, **47**, 6187–6200.
18 J. M. Recio, J. M. Menéndez and A. O. De la Roza, *An introduc-*

View Article Online
DOI: 10.1039/D2CP01266A

tion to high-pressure science and technology, CRC Press, Boca Raton, FL, USA, 2016.
19 G. Kresse and J. Furthmüller, *Comput. Mater. Sci.*, 1996, **6**, 15–50.
20 J. P. Perdew, K. Burke and M. Ernzerhof, *Phys. Rev. Lett.*, 1996, **77**, 3865–3868.
21 H. J. Monkhorst and J. D. Pack, *Phys. Rev. B*, 1976, **13**, 5188–5192.
22 P. E. Blöchl, *Phys. Rev. B*, 1994, **50**, 17953–17979.
23 G. Kresse and D. Joubert, *Phys. Rev. B*, 1999, **59**, 1758–1775.
24 A. Togo and I. Tanaka, *Scr. Mater.*, 2015, **108**, 1–5.
25 A. Otero-de-la-Roza and V. Luaña, *Comput. Phys. Commun.*, 2011, **182**, 1708–1720.
26 A. Otero-de-la-Roza, D. Abbasi-Pérez and V. Luaña, *Comput. Phys. Commun.*, 2011, **182**, 2232–2248.
27 Y. Wang, Z. T. Y. Liu, S. V. Khare, S. A. Collins, J. Zhang, L. Wang and Y. Zhao, *Appl. Phys. Lett.*, 2016, **108**, 061906 [1–5].
28 K. J. Chang and M. L. Cohen, *Phys. Rev. B*, 1987, **35**, 8196–8201.
29 K. Karch, F. Bechstedt, P. Pavone and D. Strauch, *Phys. Rev. B*, 1996, **53**, 13400–13413.
30 F. Shimojo, I. Ebbsjö, R. K. Kalia, A. Nakano, J. P. Rino and P. Vashishta, *Phys. Rev. Lett.*, 2000, **84**, 3338–3341.
31 M. Durandurdu, *Phys. Rev. B*, 2007, **75**, 235204 [1–7].
32 Y.-P. Lu, D.-W. He, J. Zhu and X.-D. Yang, *Physica B: Condensed Matter*, 2008, **403**, 3543–3546.
33 Y. Kidokoro, K. Umemoto, K. Hirose and Y. Ohishi, *Am. Mineral.*, 2017, **102**, 2230–2234.
34 H. Z. Guedda, T. Ouahrani, A. Morales-García, R. Franco, M. A. Salvadó, P. Pertierra and J. M. Recio, *Phys. Chem. Chem. Phys.*, 2016, **18**, 8132–8139.
35 K. Strössner, M. Cardona and W. Choyke, *Solid State Commun.*, 1987, **63**, 113–114.
36 M. Yoshida, A. Onodera, M. Ueno, K. Takemura and O. Shimomura, *Phys. Rev. B*, 1993, **48**, 10587–10590.
37 K. K. Zhuravlev, A. F. Goncharov, S. N. Tkachev, P. Dera and V. B. Prakapenka, *J. Appl. Phys.*, 2013, **113**, 113503 [1–12].
38 G. A. Slack and S. F. Bartram, *J. Appl. Phys.*, 1975, **46**, 89–98.
39 D. N. Talwar, *Mater. Sci. Eng. B*, 2017, **226**, 1–9.
40 Y. Fei, A. Ricolleau, M. Frank, K. Mibe, G. Shen and V. Prakapenka, *Proc. Natl. Acad. Sci. USA*, 2007, **104**, 9182–9186.
41 P. I. Dorogokupets and A. Dewaele, *High Press. Res.*, 2007, **27**, 431–446.
42 S. A. Khandy, I. Islam, D. C. Gupta, R. Khenata and A. Laref, *Scientific Reports*, 2019, **9**, 1475.
43 J. Serrano, J. Strempfer, M. Cardona, M. Schwoerer-Böhning, H. Requardt, M. Lorenzen, B. Stojetz, P. Pavone and W. J. Choyke, *Appl. Phys. Lett.*, 2002, **80**, 4360–4362.
44 B. Y. Thakore, S. G. Khambholja, A. Y. Vahora, N. K. Bhatt and A. R. Jani, *Chin. Phys. B*, 2013, **22**, 106401 [1–7].
45 V. I. Ivashchenko, P. E. A. Turchi, L. Gorb, J. Leszczynski, N. R. Medukh and R. V. Shevchenko, *J. Phys. Condens. Matter*, 2019, **31**, 405401 [1–14].
46 D. Olego and M. Cardona, *Phys. Rev. B*, 1982, **25**, 1151–1160.
47 D. Olego, M. Cardona and P. Vogl, *Phys. Rev. B*, 1982, **25**, 3878–3888.
48 N. Churcher, K. Kunc and V. Heine, *J. Phys. C Solid State Phys.*, 1986, **19**, 4413–4426.
49 B. H. Cheong, K. J. Chang and M. L. Cohen, *Phys. Rev. B*, 1991, **44**, 1053–1056.
50 W. R. L. Lambrecht, B. Segall, M. Methfessel and M. van Schilfgaarde, *Phys. Rev. B*, 1991, **44**, 3685–3694.
51 I. V. Aleksandrov, A. F. Goncharov, S. M. Stishov and E. V. Yakovenko, *JETP Lett.*, 1989, **50**, 127–131.
52 C.-Z. Wang, R. Yu and H. Krakauer, *Phys. Rev. B*, 1996, **53**, 5430–5437.
53 A. Debernardi, C. Ulrich, K. Syassen and M. Cardona, *Phys. Rev. B*, 1999, **59**, 6774–6783.
54 K. Yang, J. Xiao, J.-W. Luo, S.-S. Li, S.-H. Wei and H.-X. Deng, *New J. Phys.*, 2019, **21**, 123015 [1–9].
55 N. E. Christensen, S. Satpathy and Z. Pawlowska, *Phys. Rev. B*, 1987, **36**, 1032–1050.
56 K. Daviau and K. K. M. Lee, *Phys. Rev. B*, 2017, **95**, 134108 [1–6].
57 M. S. Miao and W. R. L. Lambrecht, *Phys. Rev. B*, 2003, **68**, 092103 [1–4].
58 K. Sarasamak, A. J. Kulkarni, M. Zhou and S. Limpijumnong, *Phys. Rev. B*, 2008, **77**, 024104 [1–12].
59 W. Lee and X. Yao, *Comput. Mater. Sci.*, 2015, **106**, 76–82.
60 X. Li and R. Jeanloz, *Phys. Rev. B*, 1987, **36**, 474–479.
61 S. J. Duclos, Y. K. Vohra and A. L. Ruoff, *Phys. Rev. B*, 1990, **41**, 12021–12028.
62 R. Paul, S. X. Hu and V. V. Karasiev, *Phys. Rev. B*, 2019, **100**, 144101 [1–16].
63 C. Li, C. Wang, J. Han, L. Yan, B. Deng and X. Liu, *J. Mater. Sci.*, 2018, **53**, 7475–7485.